

Full Research Paper

A Wetness Index Using Terrain-Corrected Surface Temperature and Normalized Difference Vegetation Index Derived from Standard MODIS Products: An Evaluation of Its Use in a Humid Forest-Dominated Region of Eastern Canada

Quazi K. Hassan^{1,*}, **Charles P.-A. Bourque**^{1,2}, **Fan-Rui Meng**¹ and **Roger M. Cox**³

1 Faculty of Forestry and Environmental Management, University of New Brunswick, Fredericton, New Brunswick, Canada E3B 6C2. E-mails: q.k.hassan@unb.ca; cbourque@unb.ca; fmeng@unb.ca

2 Lanzhou Regional Climate Centre, 2070 Donggang East Road, Lanzhou, 730020, Gansu, P.R. China.

3 Natural Resources Canada - Canadian Forest Service, Atlantic Forestry Centre, Fredericton, New Brunswick, Canada E3B 5L7. E-mail: rcox@nrcan.gc.ca.

* Author to whom correspondence should be addressed.

Received: 6 September 2007 / Accepted: 26 September 2007 / Published: 1 October 2007

Abstract: In this paper we develop a method to estimate land-surface water content in a mostly forest-dominated (humid) and topographically-varied region of eastern Canada. The approach is centered on a temperature-vegetation wetness index (TVWI) that uses standard 8-day MODIS-based image composites of land surface temperature (T_S) and surface reflectance as primary input. In an attempt to improve estimates of TVWI in high elevation areas, terrain-induced variations in T_S are removed by applying grid, digital elevation model-based calculations of vertical atmospheric pressure to calculations of surface potential temperature (θ_S). Here, θ_S corrects T_S to the temperature value to what it would be at mean sea level (i.e., ~101.3 kPa) in a neutral atmosphere. The vegetation component of the TVWI uses 8-day composites of surface reflectance in the calculation of normalized difference vegetation index (NDVI) values. TVWI and corresponding wet and dry edges are based on an interpretation of scatterplots generated by plotting θ_S as a function of NDVI. A comparison of spatially-averaged field measurements of volumetric soil water content (VSWC) and TVWI for the

2003-2005 period revealed that variation with time to both was similar in magnitudes. Growing season, point mean measurements of VSWC and TVWI were 31.0% and 28.8% for 2003, 28.6% and 29.4% for 2004, and 40.0% and 38.4% for 2005, respectively. An evaluation of the long-term spatial distribution of land-surface wetness generated with the new θ_S -NDVI function and a process-based model of soil water content showed a strong relationship (i.e., $r^2 = 95.7\%$).

Keywords: MODIS standard products, normalized difference vegetation index, surface potential temperature, soils, temperature-vegetation wetness index, vegetation, water content.

1. Introduction

Soil water content (SWC) is a measure of the total amount of water, including water vapor, contained within a column of soil above the ground water table. Water diffuses into the soil through the soil pores and is transferred through the soil at a rate defined by the soil's permeability. Available soil water is used by plant growth processes and nutrient acquisition food production (along with available light energy) and in many instances is released directly to the atmosphere through the plant-mediated processes of transpiration and evaporation of free water in the soil. SWC is a critical site variable that defines among many factors (a) the duration and intensity of drought, (b) agricultural and tree crop production and food security, (c) level of soil erosion and surface runoff impacts, and (d) rate of evapotranspiration (ET). In particular to forest-dominated regions, SWC plays a vital role in defining (a) the condition and health of forests, (b) the distribution and rate of forest growth and regeneration, (c) forest fire hazard rating, (d) level of carbon dioxide assimilation by forests, and (e) scheduling of forest harvesting and other forest management activities, such as aerial seeding and tree planting.

The most commonly used and standard protocols for estimating SWC are the "gravimetric" and "volumetric" methods. Both methods estimate SWC accurately, but only provide point measurements due to the amount of work required to process a single field sample. Automated point-sampling possible with time domain reflectometry and other electronic devices can improve the spatial coverage, but at an enormous cost. In general, field measurements of SWC are insufficient to provide the near continuous spatial coverage needed for land-management applications. As an alternative to in-field measurement of SWC, remote sensing (RS) platforms, like the TERRA satellite, can be used to generate a vast amount of information about the earth surface at resolutions small enough and frequent enough (everyday with the MODIS sensor) to be appropriate for land-management planning.

For the last two decades, optical and thermal RS sensors have been employed for estimating water content (WC) in soils and vegetation. An overview by Moran et al. [1] reveals that a strong relationship exists between WC and index values derived from surface temperature-vegetation index (T_S -VI) methods that use optical and thermal RS data as input. Although showing promise, the penetrating capabilities of optical and thermal RS sensors to sample the earth's surface diminish with the presence of clouds,

vegetation cover, and other non-transmitting surfaces. At present, many challenges remain with employing RS data in understanding earth-system processes.

The relation between T_S and VI has been previously described in scatterplots of T_S vs. VI, typically generating either “triangular” [2-3] or “trapezoidal” forms [4-5]. The edges of these forms provide the basis for modelling WC in bare soils and in vegetation (see Section 3.2 for more detail). A negative slope of the T_S -VI plot is generally observed and interpreted using micro-meteorological principles. For instance, low T_S 's generally occur over dense vegetation with high SWC, and relatively higher T_S 's, over sparse vegetation with low SWC. In the literature, T_S -VI plots have been given many different names, such as the surface moisture status [6], triangular method of indirect estimation of soil moisture [7], surface temperature-vegetation index [5], moisture index (MI; [8]), temperature-vegetation contextual (TVX; [9]), and temperature-vegetation dryness index (TVDI; [3]). The T_S -VI approach has been implemented using various RS data over a diversity of ecosystems worldwide (Table 1). The approach has also been applied in various applications, such as in quantifying (*i*) the evaporative fraction [10-11], (*ii*) ET [2, 12]), (*iii*) crop water deficit [4], (*iv*) forest fire hazard [13], and (*v*) drought duration and intensity [14].

The widely used T_S -NDVI relationship has limited application in variable topography [17]. For instance, remotely-sensed T_S can only be estimated under clear-sky conditions and T_S in variable terrain is often lower in upland areas compared to low-lying areas within the same climatic and landuse zonation. Clearly, using a response function based on strictly T_S could incorrectly suggest that land-surface conditions in upland areas are wetter than in low-lying areas. In an effort to improve WC calculations in high elevation areas, corrections are applied to T_S by applying grid, digital elevation model (DEM)-based calculations of vertical atmospheric pressure to calculations of surface potential temperature [θ_S ; 18]. Here, θ_S adjusts T_S to a value representing the temperature that would be at mean sea level (i.e., ~101.3 kPa) in a neutrally-stratified atmosphere [18].

The objectives of this paper are to: (*i*) develop a temperature-vegetation wetness index (TVWI) based on an application of an θ_S -NDVI response function constructed from MODIS-based standard products of T_S and surface reflectances; and (*ii*) evaluate the potential of TVWI to estimate both the spatial and temporal variations in SWC in a humid forest-dominated and topographically-variable landscape in eastern Canada.

Table 1. Examples of T_S -VI approaches appearing in the literature

Ref.	T_S -VI approaches used in the past*
[3]	<ul style="list-style-type: none"> Assumed variations in T_S were caused by variations in SWC; TVDI was derived from a T_S-NDVI* relation using NOAA-AVHRR images taken over Senegal in West Africa. Generally a good agreement existed between estimates of SWC from the T_S-NDVI function and estimates from hydrological models using ground-based climate data as input to the models ($r^2=70\%$).
[5]	<ul style="list-style-type: none"> Based on a trapezoidal form of the T_S-F_R* function using NOAA-AVHRR images taken over Africa. The method illustrated the conceptual borders of dry and wet soils and areas of low-to-high ET with respect to T_S and vegetation coverage.
[6]	<ul style="list-style-type: none"> Examined the effect of biome type on the slope of the T_S-NDVI function at regional and continental scales using NOAA-AVHRR images taken over western Montana, USA. The approach provided a strong relationship between the slope of the T_S-NDVI function and a crop moisture index (yielding an r^2 of 83%), pointing to the fact that the T_S-NDVI function is sensitive to surface soil water conditions.
[7, 15]	<ul style="list-style-type: none"> Represented SWC using a “triangular” approach, based on a function of T_S and NDVI using airborne images taken over the states of Kansas and Arizona, USA and processed with the SVAT* model. Method provided a standard error of 16% between T_S-NDVI wetness-value predictions and ground measurements of SWC.
[8]	<ul style="list-style-type: none"> Used T_S and a ratio of near infrared and the blue bands for modelling MI using LANDSAT images taken over northeast Brazil. Method modelled the seasonal variations of SWC due to changes in vegetation growth; correlations between MI and ground-based measurements of SWC were not reported.
[9]	<ul style="list-style-type: none"> Established relationships between the slopes of T_S-NDVI (i.e., TVX approach) and soil moisture produced with the Simplified Simple Biosphere Model using NOAA-AVHRR images taken over the HAPEX-Mobilhy site in southern France. TVX metrics provided estimates of daily soil moisture variation up to 2-cm depth in the soil and seasonal variations up to 10 cm. Method provided a general linear relation with the residual standard error of < 4% over a range of 6-27% in volumetric SWC.
[16]	<ul style="list-style-type: none"> Modelled SWC from a T_S-F_R relation using NOAA-AVHRR and LANDSAT ETM+ images taken over northeastern Spain. Method provided a reasonable agreement between NOAA and LANDSAT-based estimates of SWC ($r^2=66\%$).

***Note:** NOAA-National Oceanic and Atmospheric Administration; AVHRR-Advanced Very High Resolution Radiometer; NDVI-normalized difference vegetation index; F_R - fraction of vegetation coverage derived from NDVI; SVAT-soil vegetation atmosphere transfer model; SWC-soil water content; GMS-Geostationary Meteorological Satellite; MODIS-Moderate Resolution Imaging Spectroradiometer.

2. Study Area and Data Used

Canada is divided into fifteen terrestrial ecozones or generalized zonal groupings of similar soil formation, climate, and landuse cover [19]. In eastern Canada, the Atlantic Maritime Ecozone is dominated by forests occupying approximately three-fourths of the total ecozone's land-surface area. The combined surface area of the Provinces of New Brunswick (NB), Nova Scotia (NS), and Prince Edward Island (PEI) occupy about 80% of the total landbase of the Atlantic Maritime Ecozone. The forest in the region is generally characterized by a temperate mix wood forest of deciduous species, such as maple (*Aceraceae* spp.), beech (*Fagus grandifolia* Ehrh.) and birch (*Betulaceae* spp.), and coniferous species, such as spruce (*Picea* spp.) and balsam fir [*Abies balsamea* (L.) Mill.]. Forests occupy about 85% of NB's landbase, 79% of NS', and 46% of PEI's (Natural Resources Canada; http://cfs.nrcan.gc.ca/sof/sof06/profiles_e.html, last visited Jul. 2007). The climate in this region is largely influenced by (1) the westerly displacement of continental air masses, (2) the region's proximity to the Atlantic Ocean, and in the case of NB's southern shore and NS' northern shore, by the cold water of the Bay of Fundy, and (3) changes in elevation. The area experiences a cool-moist climate with a mean annual temperature and annual precipitation range of 3.5-6.5°C and 900-1500 mm, respectively. The Provinces of NB and NS have elevational ranges from 0-834 m for NB, and 0-540 m above mean sea level (a.s.l.) for NS. PEI is relatively flat, having an average elevation of about 30 m a.s.l. (Figure 1).

In this study, we employed 8-day composites of MODIS-based standard products of (i) daytime T_s at 1-km resolution (MOD11A2 products) and (ii) red and near infrared (NIR) surface reflectances at 250-m resolution (SR; MOD09Q1 products) obtained from NASA to generate products of NDVI at 250-m resolution. Generally, in humid, forest-dominated regions of the world day-to-day variation in SWC seldom control the long-term processes involved with defining forest productivity. As a result, WC values in this paper were calculated over 8-day intervals roughly to coincide with the 8-day standard image composites of T_s and SR. To calculate vertical atmospheric pressure variation and θ_s [18], we employed a 250-m resolution DEM of the study area generated from 3-arc second resolution height point-data acquired from the NASA Shuttle Radar Topography Mission (SRTM) archive. For comparing MODIS-derived wetness values, field measurements of volumetric soil water content (VSWC) were acquired from ten sites in southwest NB, including two Fluxnet-Canada sites [20], namely the Nashwaak Lake (NWL) and Charlie Lake (CL) sites (46° 28' 20" N, 67° 06' 00" W and 45° 53' 05" N, 67° 21' 25" W, respectively; Figure 1), and eight field sites of variable forest cover (including one bare field) on Canadian Forces Base Gagetown property (CFB; ~ 46° 40' N, 66° 22' W; Figure 1). Measurements of VSWC were obtained at all sites with water content reflectometers (i.e., CS615 or CS616 probes, Campbell Scientific Corp.) placed at 10-cm depths. To coincide with the 8-day averaging scheme employed earlier, all field measurements from the individual sites were temporally-averaged to 8-day means. Table 2 provides the time periods over which individual 8-day mean calculations of TVWI and VSWC apply. As a second comparison, we generated spatially-explicit long-term average calculations of SWC (given in "% of saturation") at 220-m resolution for the Province of NB with the well-established, process-based WET model [21-22]. Model output was calculated based on inputs of long-term average values of precipitation

(mm d^{-1}), soil infiltration capacity (mm d^{-1}), solar energy input and exchange (and, therefore, DEM; MJ d^{-1}) [23], flow accumulation (in m^2 or number of cells), and surface run-off rates (mm d^{-1}) [21-22].

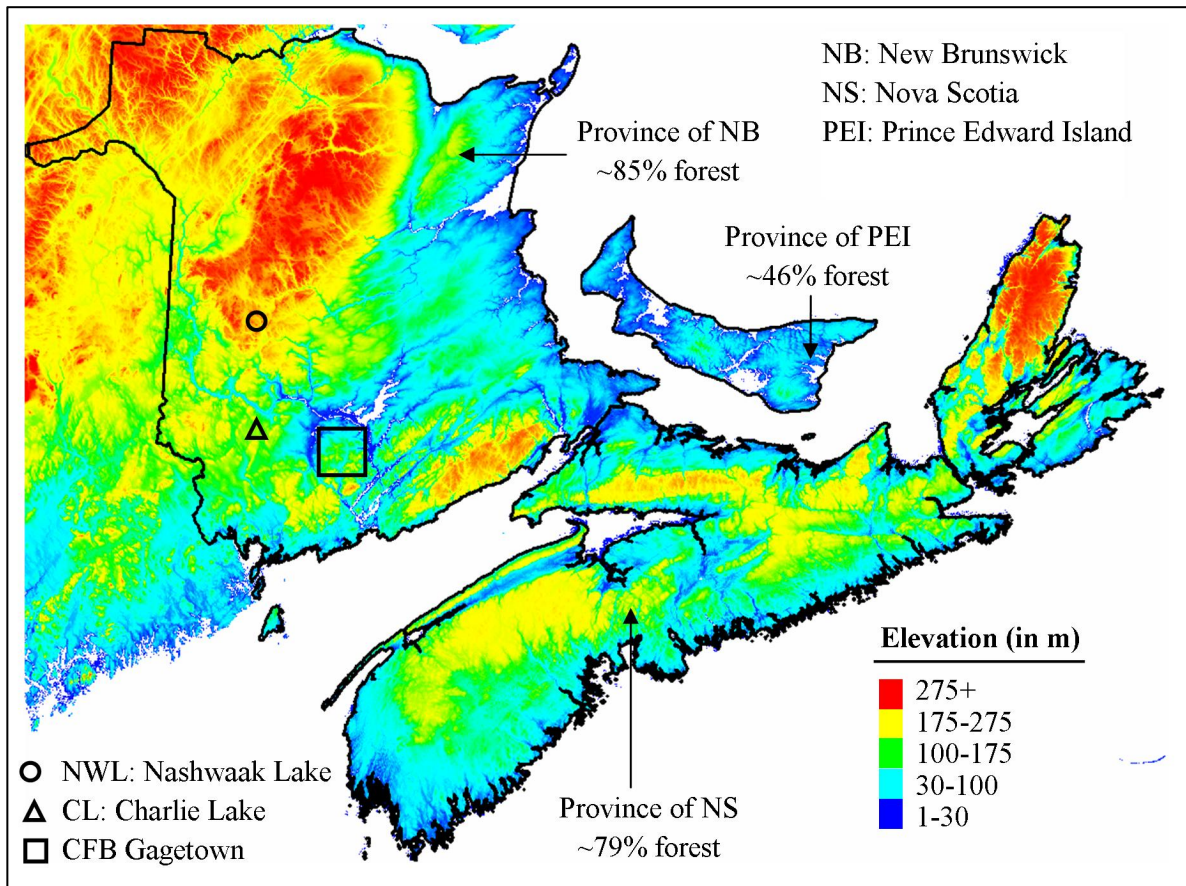


Figure 1. Study area and field locations where the measurements of volumetric soil water content were obtained. Elevations are in metres above mean sea level.

Table 2. Time periods over which the individual 8-day means were calculated.

Period no.	Day of year	Dates in 2003 and 2005	Dates in 2004	Period no.	Day of year	Dates in 2003 and 2005	Dates in 2004
1	121-128	01 May-08 May	30 Apr.-07 May	11	201-208	20 Jul.-27 Jul.	19 Jul.-26 Jul.
2	129-136	09 May-16 May	08 May-15 May	12	209-216	28 Jul.-04 Aug.	27 Jul.-03 Aug.
3	137-144	17 May-24 May	16 May-23 May	13	217-224	05 Aug.-12 Aug.	04 Aug.-11 Aug.
4	145-152	25 May-01 Jun.	24 May-30 May	14	225-232	13 Aug.-20 Aug.	12 Aug.-19 Aug.
5	153-160	02 Jun.-09 Jun.	01 Jun.-08 Jun.	15	233-240	21 Aug.-28 Aug.	20 Aug.-27 Aug.
6	161-168	10 Jun.-17 Jun.	09 Jun.-16 Jun.	16	241-248	29 Aug.-05 Sep.	28 Aug.-04 Sep.
7	169-176	18 Jun.-25 Jun.	17 Jun.-24 Jun.	17	249-256	06 Sep.-13 Sep.	05 Sep.-12 Sep.
8	177-184	26 Jun.-03 Jul.	25 Jun.-02 Jul.	18	257-264	14 Sep.-21 Sep.	13 Sep.-20 Sep.
9	185-192	04 Jul.-11 Jul.	03 Jul.-10 Jul.	19	265-272	22 Sep.-29 Sep.	21 Sep.-28 Sep.
10	193-200	12 Jul.-19 Jul.	11 Jul.-18 Jul.	20	273-280	30 Sep.-07 Oct.	29 Sep.-06 Oct.

3. Methods

Figure 2 shows a schematic diagram of the TVWI method. The method consists of (1) **data pre-processing** in the generation of the 8-day composites of NDVI and in the correction of T_S - and NDVI-image products by gap filling of cloud-contaminated pixels, (2) **calculating** θ_S and TVWI for 58 images, and (3) **performing** a comparison of TVWI with field measurements of VSWC and model calculations of SWC (“% of saturation”).

3.1. Pre-processing of the MODIS Images

Eight-day composites of NDVI were determined using:

$$NDVI = \frac{\rho_{NIR} - \rho_{red}}{\rho_{NIR} + \rho_{red}}, \quad (1)$$

where ρ is the SR values for the red and NIR bands. Cloud-contamination of pixels was identified by quality control flags contained in MOD09Q1. The 8-day datasets of T_S had clear distinction between clear-sky and cloud-contaminated pixels. To correct T_S and NDVI values for cloud-contaminated pixels, we employed an image-correction algorithm first proposed by Hassan *et al.* for the correction of T_S [24]. Mathematically, this correction is expressed as

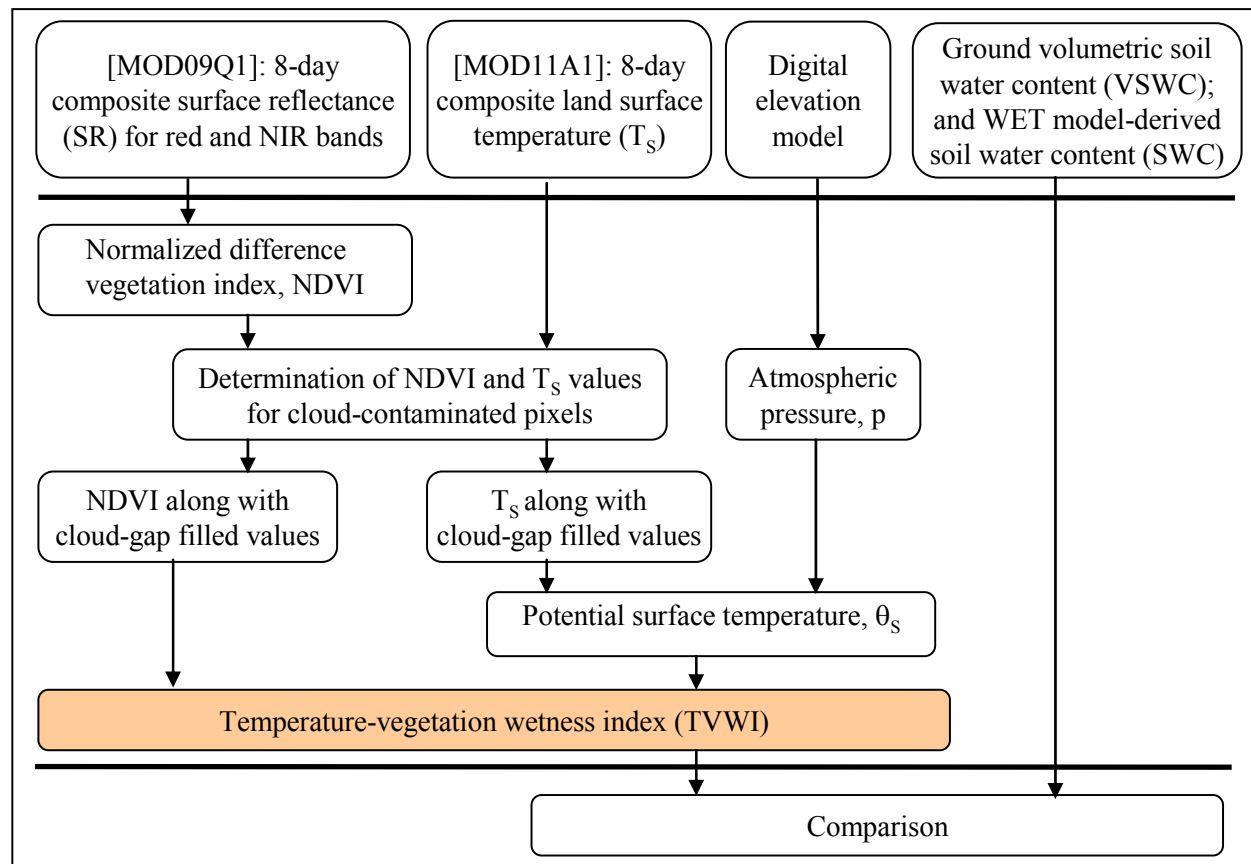


Figure 2. Schematic diagram of the TVWI method showing the steps for calculating index values of land-surface WC, and their validation with field measurements of VSWC and with WET model-generated values of “% of saturation”.

$$A = \frac{\sum_{i=1}^{i=n} \bar{X}(i) - X(i)}{m}, \text{ and} \quad (2a)$$

$$B_n = \bar{X}(n) - A, \quad (2b)$$

where $\bar{X}(i)$ is the mean value of either T_s or NDVI for each of their respective 8-day composites for a specific year (where $i=1\dots n$, and n =the total number of 8-day composite images involved per year), $X(i)$ represents the timeseries of image-based T_s and NDVI values for a specific year for cloud-contaminated pixels taking into account only T_s and NDVI values from cloud-free composites, m is the total number of cloud-free pixels from individual composite images available for a specific year for a cloud-contaminated pixel, A is the average temporal deviation of T_s and NDVI from their respective $\bar{X}(i)$'s for a specific cloud-contaminated pixel, and B_n is the estimated 8-day means of either T_s or NDVI for individual cloud-contaminated pixels.

3.2. Calculating θ_s and TVWI

There were two steps involved in the calculation of θ_s . The first step involved the calculation of atmospheric pressure (p) at each of the image pixels by referring to their respective point elevations in the acquired DEM of the study area and

$$p = 101.3 \left[\frac{293 - 0.0065z}{293} \right]^{5.26}, \quad (3)$$

[25], where p (in kPa) is the atmospheric pressure and z (in m) is the elevation a.s.l. This equation is based on a simplified form of the ideal gas law for a neutrally-stratified atmosphere and a temperature of 20°C at a standard atmosphere (i.e., 101.3 kPa). Surface potential temperature, θ_s (in K), was then calculated with

$$\theta_s = T_s \left[\frac{p_0}{p} \right]^{R/c_p}, \quad (4)$$

where T_s is the image-pixel surface temperature (in K), p_0 is the average pressure at mean sea level (set at 101.3 kPa), R is the gas constant (i.e. 287 J kg⁻¹ K⁻¹), and c_p is the specific heat capacity of air (~1004 J kg⁻¹ K⁻¹). In normal practice, meteorologists set p_0 to 100.0 kPa instead of 101.3 kPa that we used. The meteorological principles behind Eq. (4), however, remain the same.

As a result of corrections to T_s (yielding θ_s), our TVWI is based on a response function having θ_s and NDVI as the main axes. A trapezoidal shape (see Figure 3) was generally observed when θ_s and NDVI data were plotted (see Figure 5, Results & Discussion section). In Figure 3, the dry edge (θ_{dry} ; the line where θ_s is highest in relation to NDVI) represents the case where water is not available for ET, and, as a result, TVWI possesses the lowest value (~0.0). The dry edge (θ_{dry}) is determined as a linear fit of the highest θ_s in relation to NDVI. In contrast, the wet edge (θ_{wet} ; the line where θ_s is lowest in relation to NDVI; Figure 3) represents the case where water is freely available for ET and TVWI is highest (~1.0). Pixel-calculations of TVWI are based on a modified form of the wetness index proposed in [3], i.e.,

$$TVWI = \frac{\theta_{dry} - \theta_s}{\theta_{dry} - \theta_{wet}}, \quad (5)$$

where TVWI is a dimensionless quantity and θ_s , θ_{dry} and θ_{wet} are all in K.

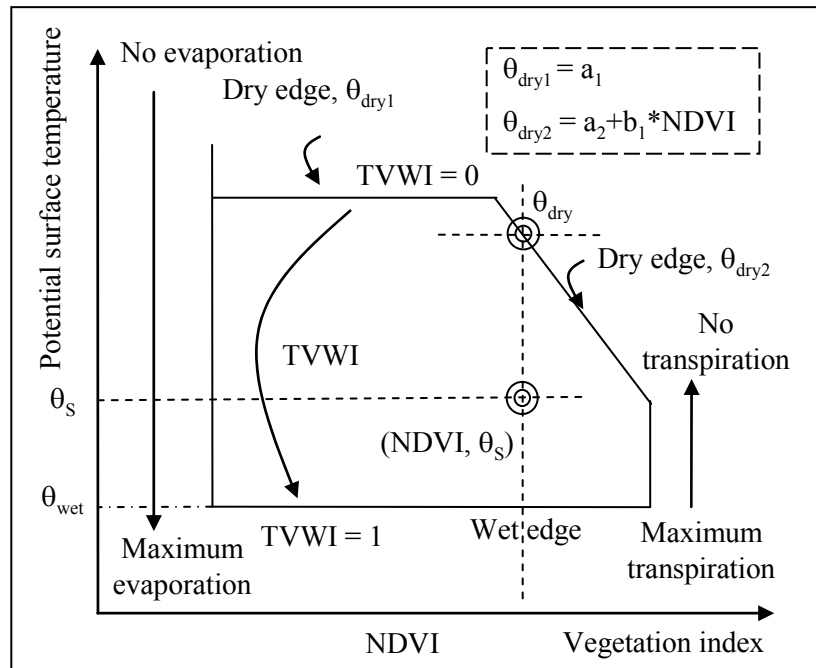


Figure 3. Trapezoidal form of the TVWI based on a relationship between θ_s and NDVI (modified after [5]). Dry and wet edges of the trapezoid are indicated.

3.3. TVWI and SWC comparisons

There were 58 TVWI maps generated for the years 2003-2005. For comparison of the calculated TVWI at the field level, we determined the point-location estimates of TVWI by (i) taking into account all TVWI-values within a 1 km \times 1 km area (representing a 4 \times 4 pixel sampling window) centered on the measurement sites, and (ii) averaging their respective values (16 in all). We analyzed the trend-lines for both the TVWI and VSWC as a function of time period (Table 2) to establish whether temporal trends between the two quantities were similar.

As a second comparison, a map of long-term averages of TVWI was created by averaging the 58 TVWI images. These values were then compared with SWC values produced with the WET model. The WET model gives SWC in “% of saturation” in the range of 0-1, with 0 to 1 representing excessively dry soil conditions to progressively wetter conditions. For each of the “% of saturation” values, we computed the mean TVWI-values from the long-term averages. Least squares regression and the coefficient of determination (r^2) were used to test the degree of agreement between the model-derived values of SWC and TVWI.

4. Results and Discussion

Figure 4a provides a verification of the gap-filling methodology for NDVI (Eq. 2) by artificially considering cloud-free pixels as cloud-contaminated and comparing their estimated NDVI values with their actual, recorded values. The study revealed that a reasonable level of agreement existed between estimated and actual NDVI values, yielding an r^2 of 82.9% and a regression slope of 0.75 resulting in a

slight over-prediction with NDVI-values < 0.75 and an under-prediction with NDVI-values > 0.75 . In a similar study of T_s , an appreciably better correlation was established; yielding $r^2=88.3\%$ and regression slope of 0.86 [24]. A possible reason for this difference may be related to the tendency of NDVI to saturate near the middle of the growing season (Figure 4b), while mean temperatures continue to vary [24]. At the point of saturation, NDVI becomes decoupled from temperature.

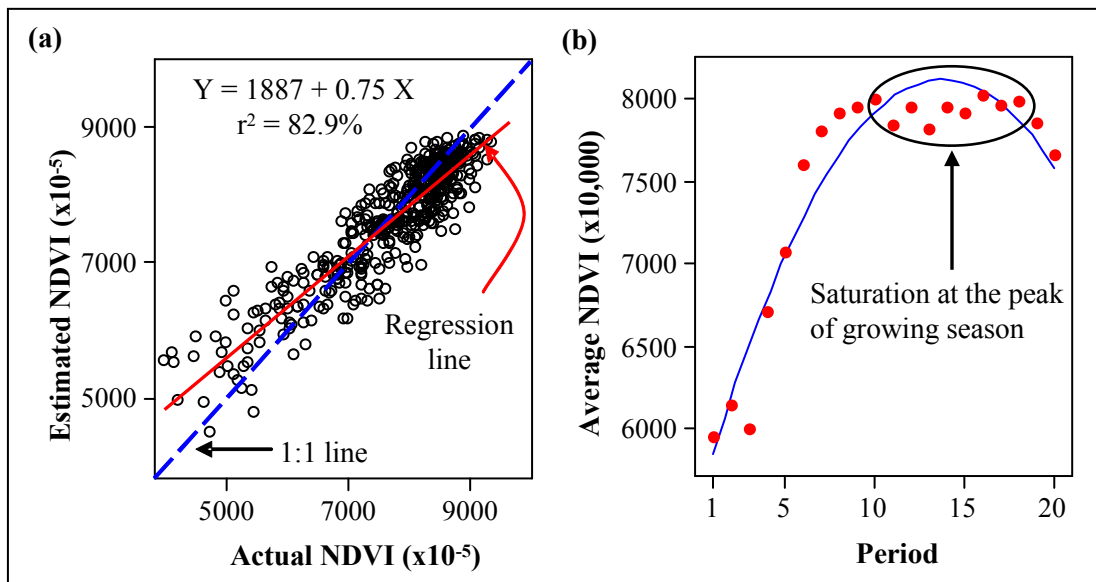


Figure 4. (a) Comparison of estimated and actual NDVI by artificially treating cloud-free pixels (cells) as cloud contaminated; and (b) seasonal pattern of spatially-averaged NDVI for the 2003-2005 period.

Figure 5 shows some example scatterplots (and related dry and wet edges) obtained by plotting θ_s against NDVI. Among the cases considered, all scatterplots matched Figure 3, although slight differences in dry and wet edges were observed. Despite θ_{wet} varied among periods (with a range of 268-282 K), we used a constant mean value of 275 K for θ_{wet} to calculate variations in TVWI. The rationale behind this strategy was to ensure that: (i) the same baseline was used to find the maximum TVWI (i.e., 1.0) across the entire series of images, and (ii) the value of $\theta_{wet} \geq 275$ was sufficiently high to support ET.

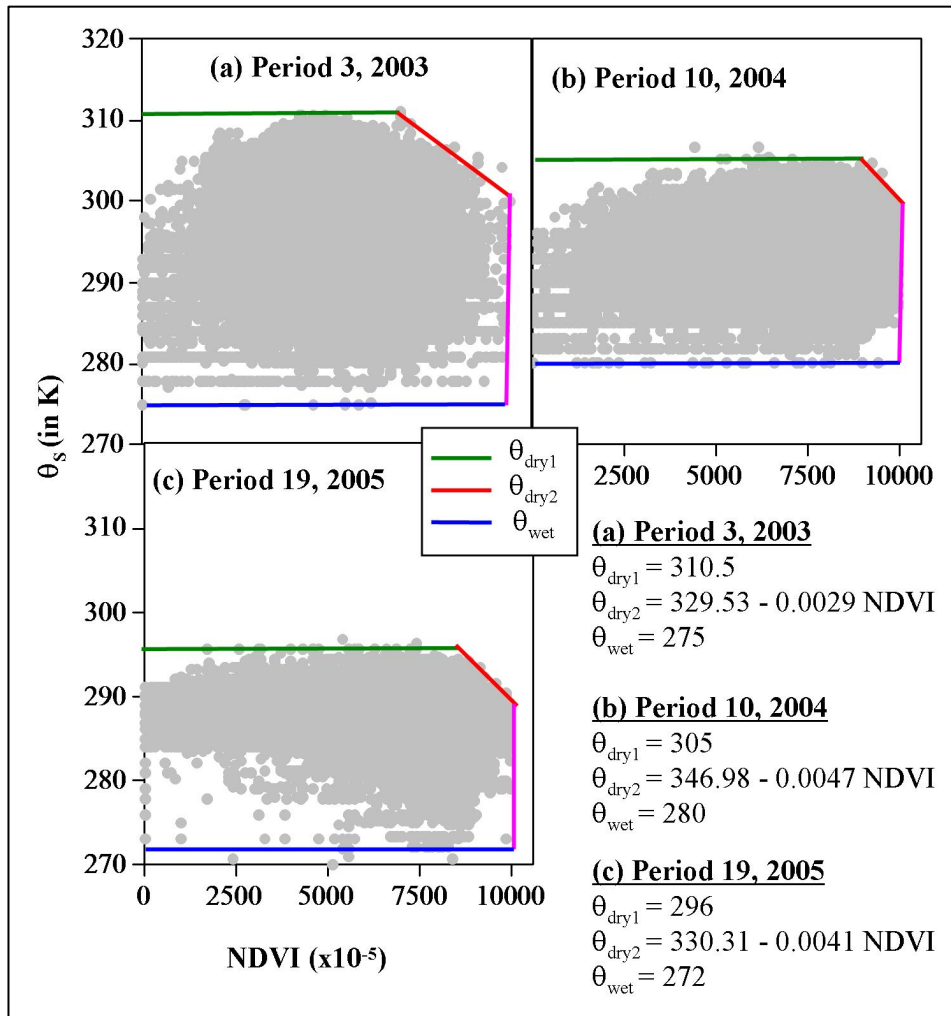


Figure 5. Example scatterplots of θ_s vs. NDVI and delineation (definition) of related dry and wet edges (following Figure 3).

Figure 6 shows the spatiotemporal variability of VSWC and derived TVWI specifically for the field sites (i.e., at NWL, CL, and CFB Gagetown in Figure 1). For each period of 2003-2005 (Table 2), we generated a pair of box-plots to demonstrate the spatial variability among sites. In general, a larger spatial variability was observed in VSWC compared to TVWI. This was expected given VSWC was acquired at point locations, while TVWI values were obtained by averaging individual pixel values within a 1 km × 1 km area centered over the point of measurement. The mean values represented by the red and blue closed symbols in Figure 6, however, were consistently close (within $\sim \pm 25\%$ or better).

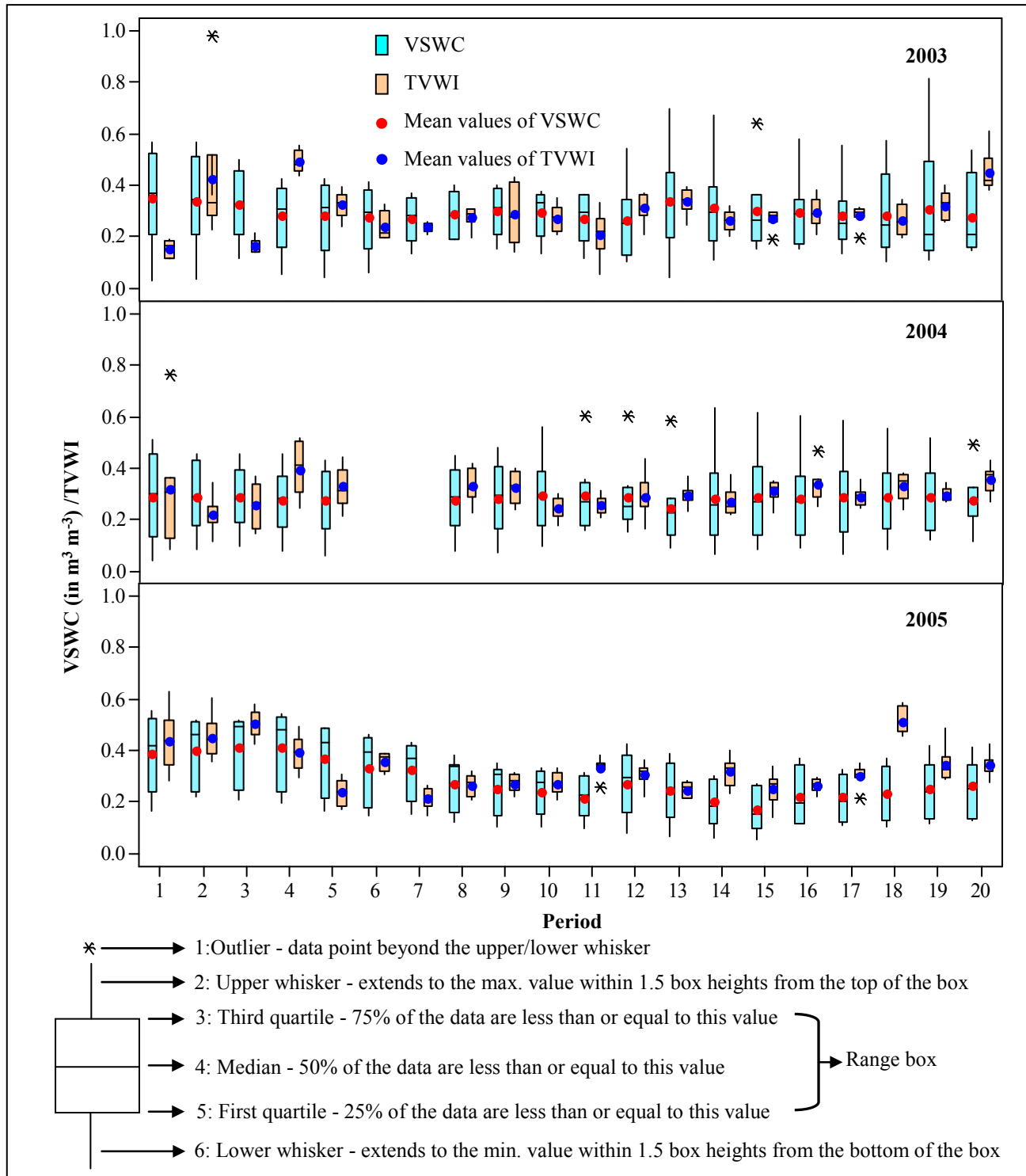


Figure 6. Box plots of spatiotemporal variation in volumetric soil water content (VSWC) and TVWI for the 2003-2005 period.

Figure 7 provides the mean trends of VSWC and TVWI for individual years. In this analysis, we discarded two values, i.e., the value for period 20 of 2003 and period 18 of 2005 (Figure 7). During the

affected period in 2003, we found T_S to suddenly drop, which caused TVWI to rise above normal conditions and become somewhat unrepresentative. In 2005, the 8-day T_S composite for that period over the field sites (Figure 1) were generated using one to three days of T_S data as a result of excessive cloudiness, which may have provided an unrepresentative calculation of T_S and, therefore, TVWI. Apart from these two apparent anomalies, our analysis revealed that the temporal trend lines for VSWC and TVWI were fairly close to each other (Figure 7). The y-intercepts of VSWC and TVWI trend lines indicated a fairly consistent relationship between mean quantities, i.e., 31.0% and 29.0% for 2003, 28.6% and 29.4% for 2004, and 40.0% and 38.4% for 2005; with all slopes near 0.0 except for 2005. In 2003 and 2004, *mean* VSWC and TVWI values were nearly identical and mostly stable during the growing period ($|\text{slopes}| \leq 0.001$), whereas those in 2005 were high at the beginning (~ 0.38) and subsequently decreased in successive periods (slope of ~ -0.01 : Figure 7).

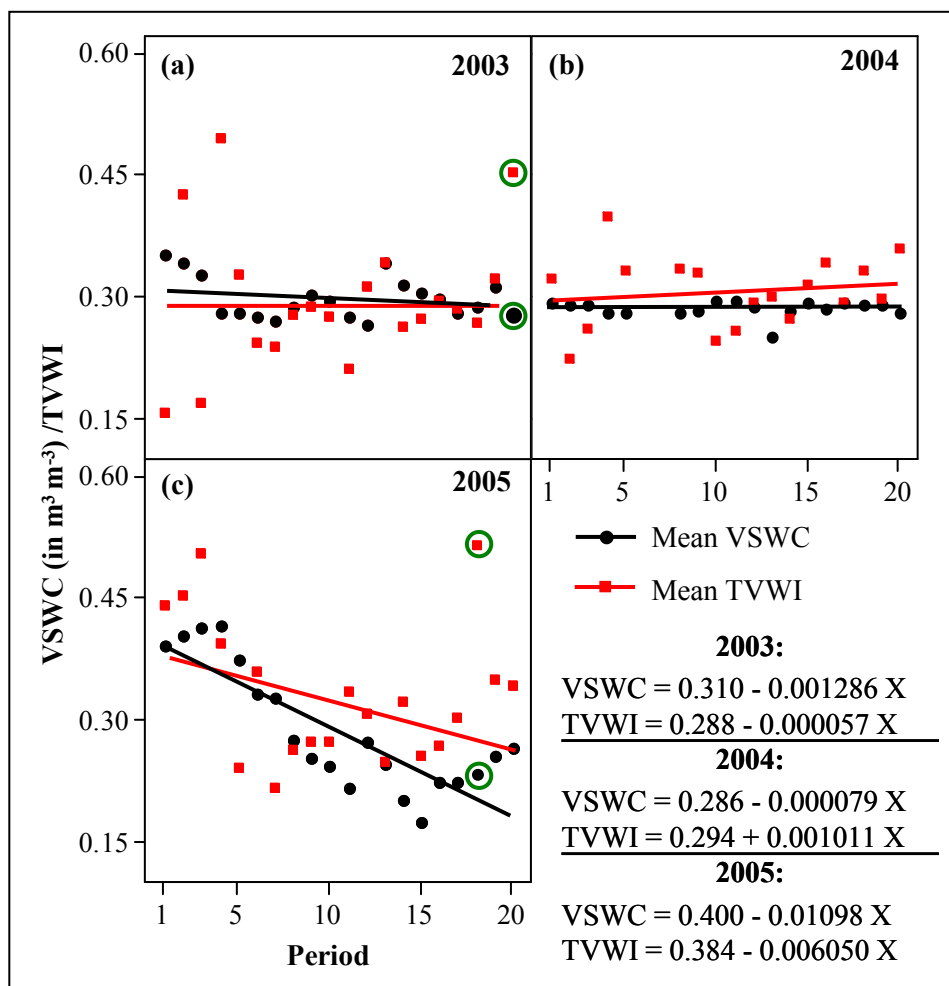


Figure 7. Comparison of mean volumetric soil water content (VSWC) and TVWI values as a function of time period (see Table 2, for actual dates). Circled symbols in panels (a) and (c) represent anomalous data removed from trend analysis (see main text for details).

Figure 8 shows the interannual variation of monthly total rainfall over the months of April to September, 2003-2005. In 2003 and 2004, VSWC and TVWI values were fairly stable over the growing period (Figure 7); most likely as a result of the near uniform distribution of rainfall over the growing season. Slight increases in rainfall in the months of September in 2003 and August in 2004 were to some extent reflected in small increases in plotted VSWC and TVWI values (with mostly increases in TVWI, in 2004) during the latter part of the season (periods 13-15 in 2003, and 15-20 in 2004; Figure 7). In 2005, early in the season both VSWC and TVWI (mean and plotted values) were high. This is mostly a reflection of the higher rainfall in April and May, coupled with the release of meltwater early in the spring. Apart from the month of June, the other months in 2005 had sufficiently high amounts of rainfall. Added rainfall in the latter part of the season in 2005 (time periods 10-20) resulted in increases in both plotted VSWC and TVWI values (but mostly in TVWI values; Figure 7), despite an overall downward mean projection suggested by linear regression. Although rainfall is one of the primary controls affecting increases in SWC, other factors like drainage, soil infiltration capacity, surface runoff, deep percolation, soil-vegetation-atmospheric interactions that also influence VSWC and TVWI dynamics, often make interpretation of figures like Figure 7 difficult.

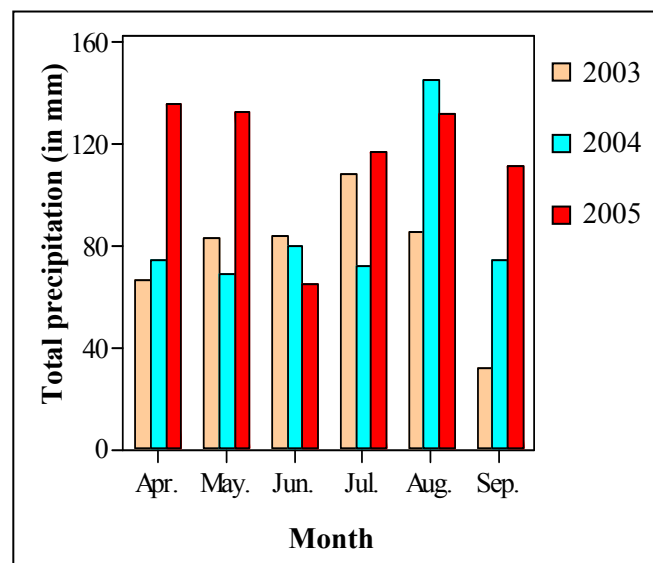


Figure 8. Monthly total rainfall over April through to September, 2003-2005. Values are based on averaging rainfall measurements taken at weather stations in proximity to the field sites (Figure 1), namely, the Fluxnet-Canada sites, Juniper, Woodstock, and CFB Gagetown Environment Canada weather stations.

From this analysis, TVWI (on the basis of relations between θ_s and NDVI) could be perceived as an indirect measure of SWC because of the following reasons:

- (i) The TVWI values were extremely close to VSWC values in terms of their magnitudes, even in heavily-forested areas (see Figure 7).
- (ii) As TVWI is based on the measure of surface properties, TVWI could be viewed as an indirect indicator of canopy (overstory foliage) WC. Canopy foliage WC in normal conditions is in equilibrium with SWC due to the relation between the water balance and total leaf area index [26]. This equilibrium could proceed uninterrupted if plant growth is unaffected by disturbance agents such as disease, insect infestation, physiological drought caused by soil-water logging or disruption of root to shoot ratios by air pollutant deposition [27-28] or winter conditions such as prolonged winter thaws [29]. Moreover, plant water potential (a measure of in-canopy WC) and soil water potential (an indirect measure of SWC) were shown to be strongly correlated [30-31]. In humid, water surplus conditions it is expected that ET would proceed at sufficiently elevated rates to cause measurable cooling of the immediate environment; on average, $\sim 2/3$ of available net radiation goes to ET in water surplus areas of the world [32].

Figure 9a provides a map of long-term averages of TVWI produced by averaging the 58 TVWI images. TVWI values fell mostly in the range of 20-60% with an average of 40%. In summary:

- (i) The areas along the coastlines and wider river channels showed higher TVWI, $> 50\%$, due to their proximity to water and low elevation relative to exposed water.
- (ii) Some high relief areas, such as in northwestern NB and in the eastern part of NS, had comparatively lower TVWI values than other regions in the Maritime Provinces (20-32%). A similar pattern was observed with “% of saturation” values generated with the WET model for the Province of NB, despite some minor differences in low-lying areas of the Province (Figure 9c).
- (iii) A comparison of mean values of TVWI with values of “% of saturation” for the same pixels and region provided reasonable agreement ($r^2=95.7\%$; Figure 10a); indicating that for the most part (for $> 99.5\%$ of the values) the wetness distributions in Figures 9a and 9c for the Province of NB, despite having different wetness units (Figures 9b and 10b), were mostly the same. Values of “% of saturation” < 0.45 were not included in the comparison as (i) the mean TVWI values did not show any clear pattern with modelled wetness values (Figure 10a), and (ii) the amount of data involved was fairly small, comprising $< 0.5\%$ of total available data points (Figure 10b). Reasons for divergence in the low “% of saturation” range (Figure 10a) remain unknown to us.

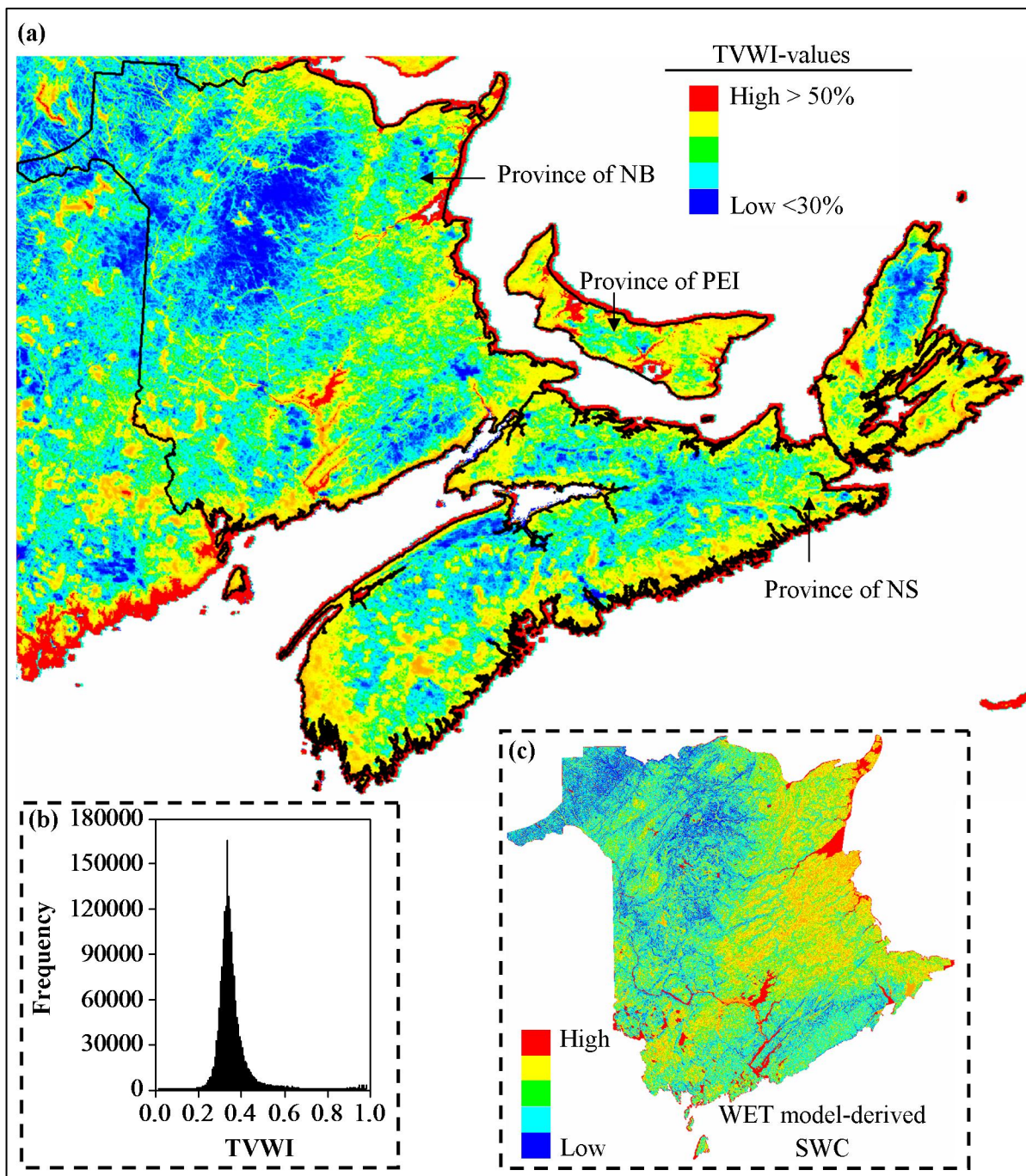


Figure 9. (a) Spatial distribution of long-term averages of TVWI at 250-m resolution, (b) frequency distribution of TVWI values, and (c) WET-generated long-term averages of “% of saturation” for the Province of NB at 220-m resolution.

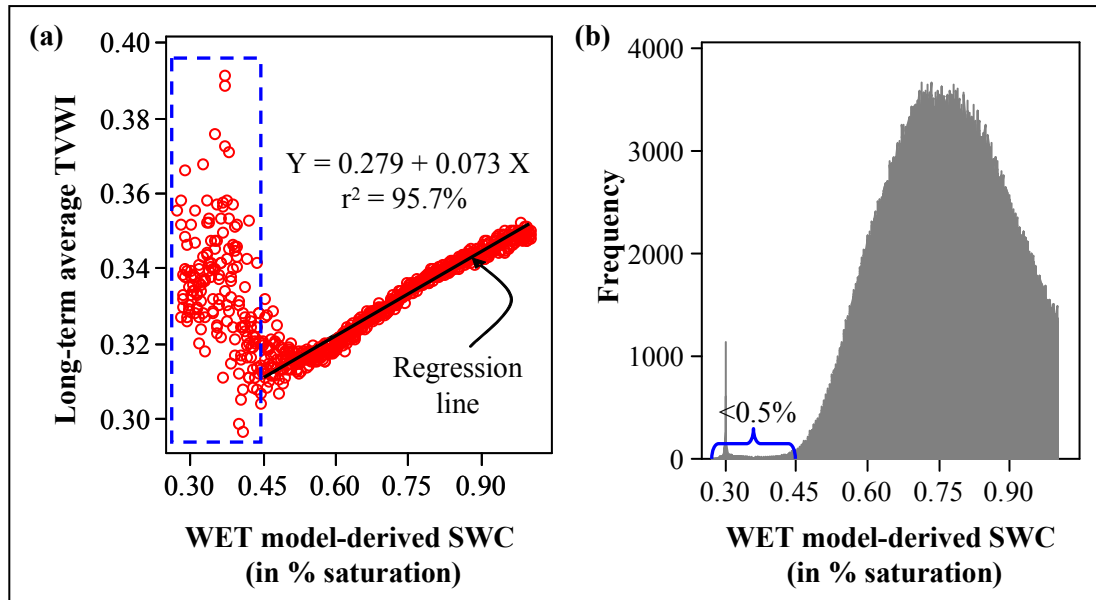


Figure 10. (a) Comparison of WET-generated “% of saturation” with long-term averages of TVWI, and (b) frequency distribution of “% of saturation” values appearing in Figure 9c. The extended left-hand tail of the frequency distribution in (b) and boxed data points in (a) accounts for < 0.5% of all available data points.

5. Concluding Remarks

In this paper, we demonstrated a practical way to estimate the spatiotemporal variability in surface wetness conditions in a forest-dominated, topographically-diverse region of eastern Canada using MODIS data. Here, the wetness index (TVWI) is based on a function of θ_s -NDVI obtained by processing standard MODIS-based products of 8-day composites of surface temperature and surface reflectance. The use of θ_s in the calculation of TVWI provides a novel approach to dealing with terrain-induced variation in temperature and, therefore, TVWI and surface-wetness mapping from satellite optical and thermal imaging of forested landscapes. In order to calculate θ_s , we apply a correction to surface temperatures by employing basic principles of meteorology. The TVWI developed here was shown to capture a significant portion of (i) the spatiotemporal variability in field measurements of SWC at ten, mostly forested sites in southwest NB, and (ii) the spatial variability in modelled values of “% of saturation” generated for the Province of NB. The TVWI can be viewed as an indirect measure of SWC as surface vegetation water content in normal, humid conditions has been previously shown by others to be mostly in equilibrium with SWC.

Acknowledgements

This study was partially funded by Fluxnet Canada Research Network (FCRN) with funds from the Natural Science and Engineering Council of Canada (NSERC), the Canada Foundation of Climate and Atmospheric Sciences (CFCAS), BIOCAP Canada Foundation, and funds from a Discovery Grant awarded to CPAB by NSERC. We would like to acknowledge NASA for providing MODIS and DEM

point data free of charge. We would also like to thank Mr. Don Coleman, Meteorological Service of Canada, for providing measurements of SWC at field sites managed by CFB Gagetown personnel. Partial financial support was provided to QKH through the “Dorothy and Kenneth Langmaid Forest Soils and Tree Growth Scholarship” administered by the Fundy Community Foundation of NB, Canada.

References and Notes

1. Moran, M.S.; Peters-Lidard, C.D.; Watts, J.M.; and McElroy, J. Estimating soil moisture at the watershed scale with satellite-based radar and land surface models. *Can. J. Remote Sens.* **2004**, *30*, 805–826.
2. Nemani, R.; Running, S. Estimation of regional surface resistance to evapotranspiration from NDVI and thermal-IR AVHRR data. *J. Appl. Meteor.* **1989**, *28*, 276-284.
3. Sandholt, I.; Rasmussen, K.; Andersen, J. A simple interpretation of the surface temperature/vegetation index space for assessment of surface moisture status. *Remote Sens. Environ.* **2002**, *79*, 213-224.
4. Moran, M.S.; Clarke, T.R.; Inoue, Y.; Vidal, A. Estimating crop water-deficit using the relation between surface-air Temperature and spectral vegetation index. *Remote Sens. Environ.* **1994**, *49*, 246-263.
5. Lambin, E.F.; Ehrlich, D. The surface temperature -vegetation index space for land cover and land-cover change analysis. *Int. J. Remote Sens.* **1996**, *17*, 463–487.
6. Nemani, R.; Pierce, L.; Running, S.; Goward, S. Developing satellite-derived estimates of surface moisture status. *J. Appl. Meteor.* **1993**, *32*, 548–557.
7. Carlson, T.N.; Gillies, R.R.; Schmugge, T.J. An interpretation of methodologies for indirect measurement of soil water content. *Agric. and For. Meteor.* **1995**, *77*, 191–205.
8. Dupigny-Giroux, L.; Lewis, J.E. A moisture index for surface characterization over a semiarid area. *Photo. Eng. & Remote Sens.* **1999**, *65*, 937–946.
9. Goward, S.N.; Xue, Y.; Czajkowski, K.P. Evaluating land surface moisture conditions from the remotely sensed temperature/vegetation index measurements: an exploration with the simplified simple biosphere model. *Remote Sens. Environ.* **2002**, *79*, 225–242.
10. Jiang, L.; Islam, S. Estimation of surface evaporation map over southern Great Plains using remote sensing data. *Water Resour. Res.* **2001**, *37*, 329-340.
11. Nishida, K.; Nemani, R.R.; Glassy, J.M.; Running, S.W. Development of an evapotranspiration index from Aqua/MODIS for monitoring surface moisture status. *IEEE Trans. Geosci. and Remote Sens.* **2003**, *41*, 493- 501.
12. Hassan, Q.K.; Bourque, C.P.-A. Estimating daily evapotranspiration for forests in Atlantic Maritime Canada: application of MODIS imagery. In *Proc. ASPRS*, 2006, 11p. CD-ROM unpaginated.
13. Vidal, A.; Devaux-Ros, C. Evaluating forest fire hazard with a Landsat TM derived water stress index. *Agric. and For. Meteor.* **1995**, *77*, 207-224.

14. Wang, C.; Qi, S.; Niu, Z.; Wang, J. Evaluating soil moisture status in China using the temperature–vegetation dryness index (TVDI). *Can. J. Remote Sens.* **2004**, *30*, 671–679.
15. Gilles, R.R.; Carlson, T.N.; Cui, J.; Kustas, W.P.; Humes, K.P. Verification of the triangle method for obtaining surface soil water content and energy fluxes from remote measurements of Normalized Difference Vegetation Index (NDVI) and surface radiant temperature. *Int. J. Remote Sens.* **1997**, *18*, 3145–3166.
16. Vicente-Serrano, S.M.; Pons-Fernández, X.; Cuadrat-Prats, J.M. Mapping soil moisture in the central Ebro river valley (northeast Spain) with Landsat and NOAA satellite imagery: a comparison with meteorological data. *Int. J. of Remote Sens.* **2004**, *25*, 4325–4350.
17. Carlson, T. An overview of the "triangle method" for estimating surface evapotranspiration and soil moisture from satellite imagery. *Sensors* **2007**, *7*, 1612–1629.
18. Rogers, R.R.; Yau, M.K. *A short course in cloud physics*; Butterworth-Heinemann: Woburn, MA, USA, 3rd edition, 1989, 304p.
19. Ecological Stratification Working Group. *A National Ecological Framework for Canada*. Agriculture and Agri-Food Canada, Research Branch, Centre for Land and Biological Resources Research and Environment Canada, State of Environment Directorate, Ottawa/Hull, 1996, 125p.
20. Coursolle, C.; Margolis, H.A.; Barr, A.G.; Black, T.A.; Amiro, B.D.; McCaughey, J.H.; Flanagan, L.B.; Lafleur, P.M.; Roulet, N.T.; Bourque, C.P.-A.; Arain, M.A.; Wofsy, S.C.; Dunn, A.; Morgenstern, K.; Orchansky, A.L.; Bernier, P.Y.; Chen, J.M.; Kidston, J.; Saigusa, N.; Hedstrom, N. Late-summer carbon fluxes from Canadian forests and peatlands along an east–west continental transect. *Can. J. For. Res.* **2006**, *36*, 783–800.
21. Moore, I.D.; Norton, T.W.; Williams, J.E. Modelling environmental heterogeneity in forested landscapes. *J. Hydrology* **1993**, *150*, 717–747.
22. Gallant, J. Complex wetness index calculations, WET documentation version 2.0. Centre for Resource and Environmental Studies, Australian National University, Canberra, 1996.
23. Bourque, C.P.-A.; Meng, F.R.; Gullison, J.J.; Bridgland, J. Biophysical and potential vegetation growth surfaces for a small watershed in northern Cape Breton Island, Nova Scotia, Canada. *Can. J. For. Res.* **2000**, *30*, 1179–1195.
24. Hassan, Q.K.; Bourque, C.P.-A.; Meng, F.-R.; Richards, W. Spatial mapping of growing degree days: an application of MODIS-based surface temperatures and enhanced vegetation index. *J. Appl. Remote Sens.* **2007**, *1*, 013511 (12p.)
25. Allen, R.G.; Pereira, L.S.; Raes, D.; Smith, M. Crop evapotranspiration: guide-lines for computing crop water requirements. Food and Agriculture Organizations of the United Nations, Rome, Italy, 1998, ISBN 92-5-104219-5. 290p.
26. Grier, C.C.; Running, S.W. Leaf area of mature northwestern coniferous forests: relation to site water balance. *Ecology* **1977**, *58*, 893–899.
27. Rennenberg, H.; Herschbach, C.; Polle, A. Consequences of air pollution on shoot-root interactions. *J. Plant Physiology* **1996**, *148*, 296–301.

28. Persson, H.; Majdi, H. Effects of acid deposition on tree roots in Swedish forest stands. *Water Air Soil Pollution* **1995**, *85*, 1287-1292.
29. Bourque, C.P.-A.; Cox, R.M.; Allen, D.J.; Arp, P.A.; Meng, F.-R. Spatial extent of winter thaw events in eastern North America: historical weather records in relation to yellow birch decline. *Global Change Biology* **2005**, *11*, 1477-1492.
30. Pabst, R.J.; Tappeiner II, J.C.; Newton, M. Varying densities of Pacific madrone in a young stand in Oregon alter soil water-potential, plant moisture stress, and growth of Douglas fir,” *For. Ecology & Management* **1990**, *37*, 267-283.
31. Fotelli, M.N.; Geßler, A.; Peuke, A.D.; Rennenberg, H. Drought affects the competitive interactions between *Fagus sylvatica* seedlings and an early successional species, *Rubus fruticosus*: responses of growth, water status and $\delta^{13}\text{C}$ composition. *New Phytologist* **2001**, *151*, 427-435.
32. Oke, T.R. *Boundary layer climates*; Routledge, London, UK, 2nd edition, 1987, 464p.